Electronic Supplementary Material (ESI) for Dalton Transactions

Supporting Information

Efficient red emission from PMMA films doped with 5,6-DTFI europium(III) complexes:synthesis, structure and photophysical properties

Weizuo Li, Pengfei Yan,* Guangfeng Hou, Hongfeng Li and Guangming Li*

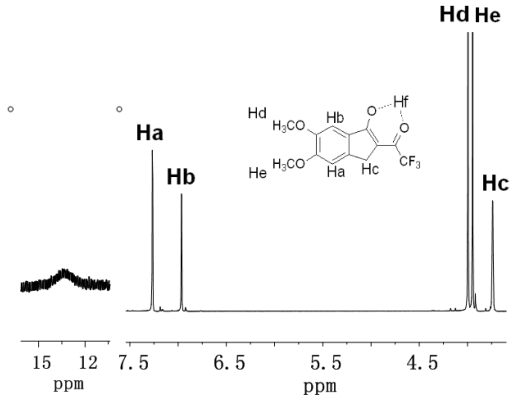

Fig. S1 400 MHz ^{1}H NMR spectrum of 5,6-DTFI in $CDCl_3$.

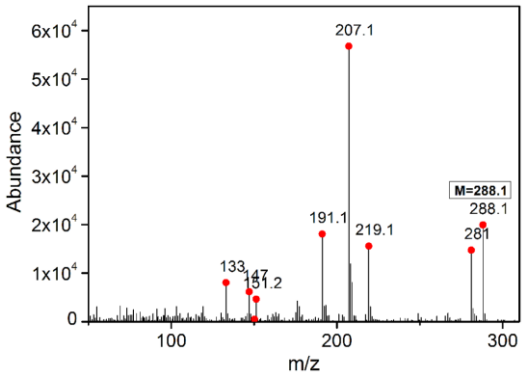

Fig. S2 Expanded regions of the EI-MS of 5,6-DTFI in acetone.

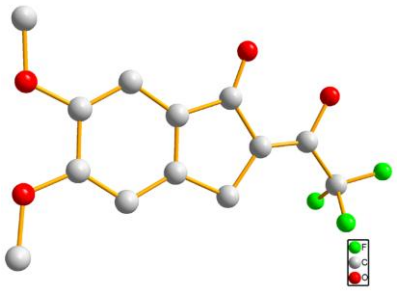

Fig. S3 Molecular structure of 5,6-DTFI.

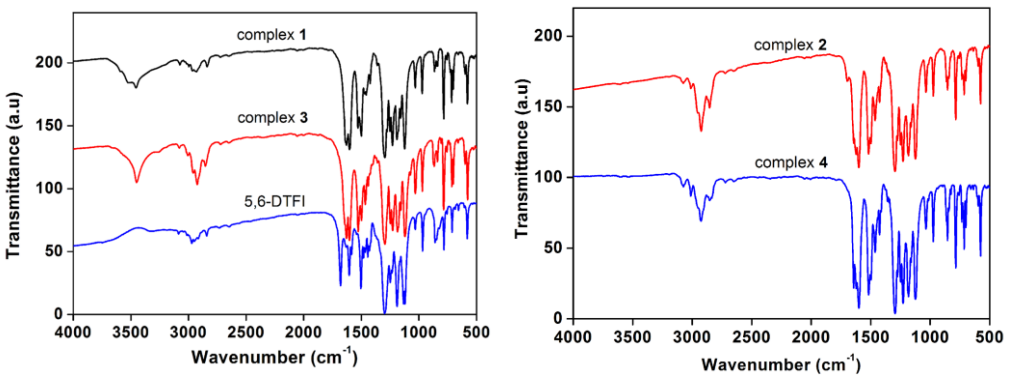

Fig. S4 IR spectra of 5,6-DTFI, complexes **1** and **3** (left); IR spectra of complexes **2** and **4** (right).

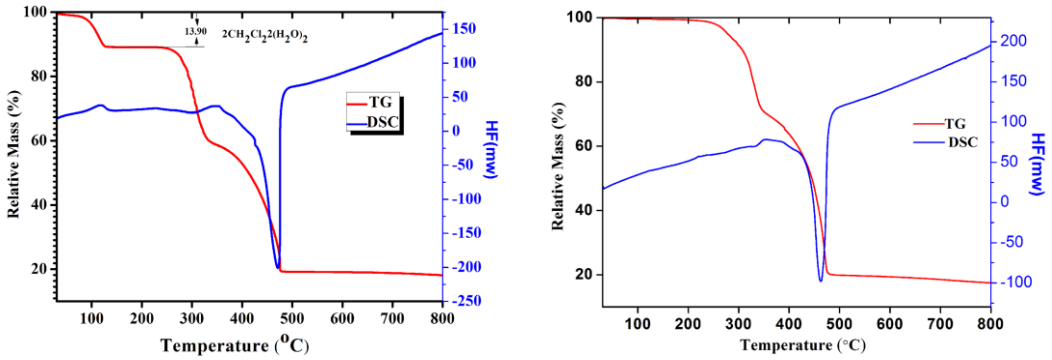

Fig. S5 TG-DSC curve for complexes **1**(left) and **2** (right).

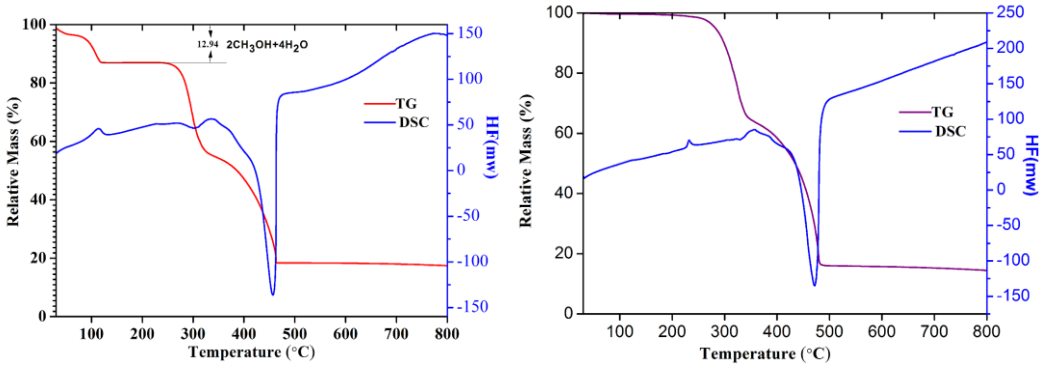

Fig. S6 TG-DSC curve for complexes **3** and **4**.

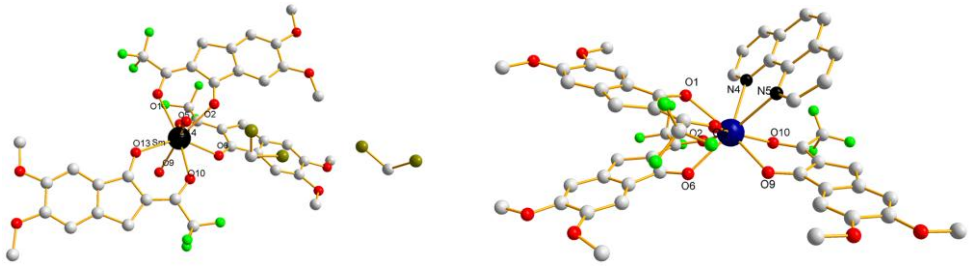

Fig. S7 Molecular structure of complexes **3** and **4**.

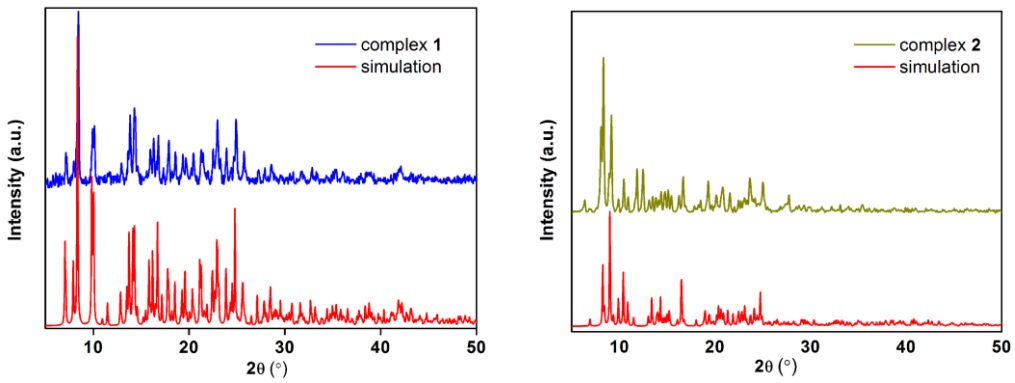

Fig. S8 X-ray powder pattern of microcrystalline samples and simulated patterns of **1** and **2**.

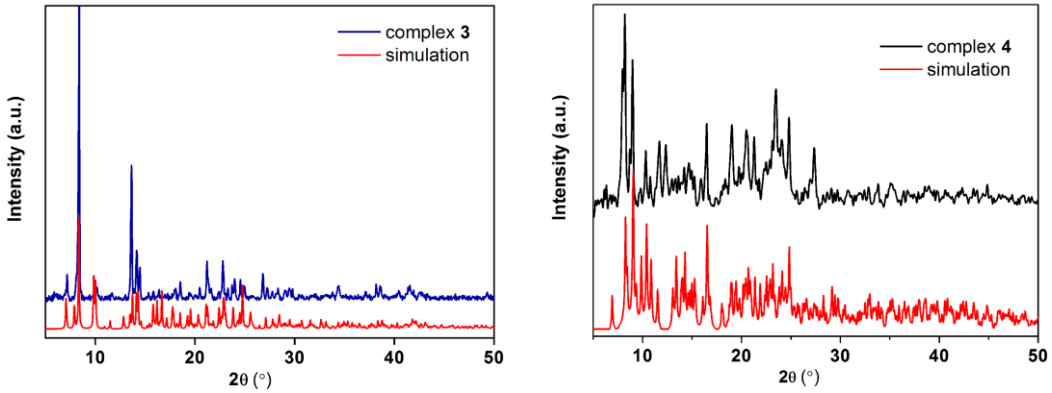

Fig. S9 X-ray powder pattern of microcrystalline samples and simulated patterns of **3** and **4**.

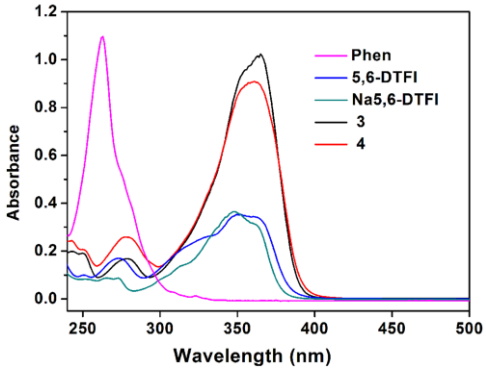

Fig. S10 UV–vis absorption spectra of 5,6-DTFI, Na5,6-DTFI, Phen, complexes **3** and **4** in CH_3CN solution ($c = 1 \times 10^{-5}$ M).

Solution-state luminescent properties of complexes 1–4

The excitation and emission spectra of **1** and **2** in CH_3CN solution ($c = 1 \times 10^{-5}$ M) are shown in (Fig. S11 left). The excitation spectra of complexes **1** and **2** exhibit a broad band between 230 and 420 nm which is due to the π-π* transition of the coordinated ligand. This result indicates that the emission of the Eu^{3+} complexes are mainly sensitized by the absorption of the β-diketone ligand in the UV region rather than directly by the Eu^{3+} ion absorption. Upon excitation at 375 nm, complexes **1** and **2** showed the characteristic narrow emission bands of the Eu^{3+} ion corresponding to the $^5D_0 \rightarrow {}^7F_J$ (J = 0–4)

transitions. Among them, the $^5D_0 \rightarrow {}^7F_2$ transition at λ = 612 nm is the strongest that is an induced electric dipole transition and its corresponding intensity is very sensitive to the coordination environment. This very intense $^5D_0 \rightarrow {}^7F_2$ peak, pointing to a highly polarizable chemical environment around the Eu^{3+} ion and is responsible for the brilliant red emission of complexes **1** and **2**.

The excitation and emission spectra of **3** and **4** in CH_3CN solution (c = 1 × 10^{-5} M) are displayed in (Fig. S11 right) The excitation spectra of complexes **3** and **4** exhibit two bands between 230–350 nm and 380–430 nm, which are due to the π-π* transition of the coordinated ligand. PL spectra of complexes **3** and **4** in CH_3CN shows typical narrow band emissions of Sm^{3+} ion corresponding to the $^4G_{5/2} \rightarrow {}^6H_J$ (J = 5/2, 7/2, 9/2, 11/2) transitions. The three expected peaks for the $^4G_{5/2} \rightarrow {}^6H_{5/2-9/2}$ transitions are well resolved. The most intense peak is the hypersensitive transition $^4G_{5/2} \rightarrow {}^6H_{9/2}$ at 645 nm.

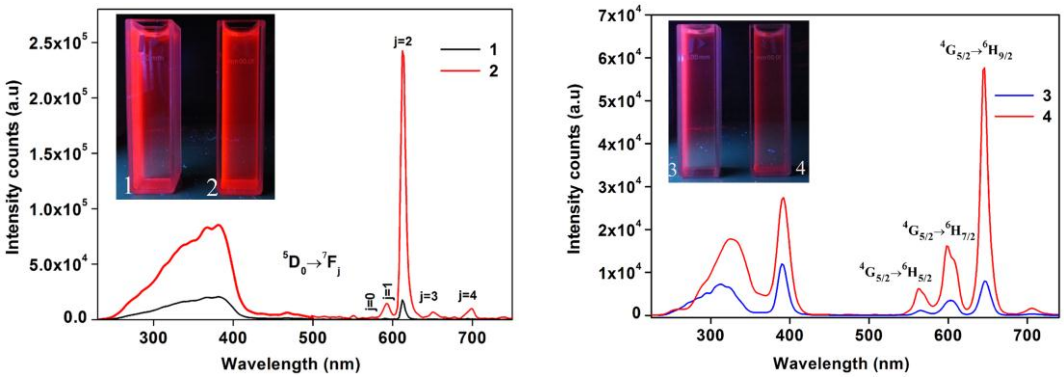

Fig. S11 Room temperature (298K) excitation and emission spectra of complexes **1** and **2** in CH_3CN solution (c = 1 × 10^{-5} M) (left); Room temperature (298K) excitation and emission spectra of complexes **3** and **4** in CH_3CN solution (c = 1 × 10^{-5} M) (right).

The luminescence decays (τ_{obs}) are single exponential functions for complexes **1** and **2** at 298 K in acetonitrile solution (c = 1 × 10^{-5} M) (Fig. S12 left)., The shorter lifetime observed for complex **1** (τ_{obs} = 26.52 μs) belongs to the dominant non-radiative decay channels associated with vibronic coupling induced by the presence of water molecules. On the other side, because of the disappeared of non-radiative decay pathways, longer lifetime values have been observed for complex **2** (τ_{obs} = 219.33 μs) due to the phen replace the water molecules of complex **1**.

The luminescent decay profiles of the $^4G_{5/2} \rightarrow {}^6H_{9/2}$ transition at 645 nm for complexes **3** and **4** in acetonitrile solution (c = 1 × 10^{-5} M) at 298K (Fig. S12 right). The luminescent decay profiles for complexes **3** and **4** at 298K by fitting the data to a single-exponential decay curve. The relatively shorter lifetime observed for complex **3** (τ_{obs} = 9.43 μs) can be caused by dominant nonradiative decay channels associated with vibronic coupling because of the presence of water molecules, On the other hand, the relative longer lifetime have been observed for complex **4** (τ_{obs} = 28.13 μs) dues to the less important nonradiative deactivation pathways.

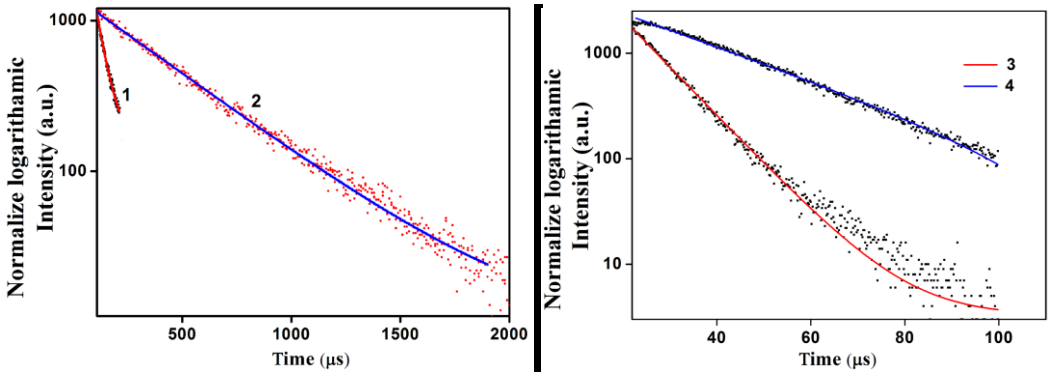

Fig. S12 Luminescence decay profiles for complexes **1**−**2** (left) and **3**−**4** (right) in CH_3CN solution ($c = 1 \times 10^{-5}$ M) were measured at 298K.

Table S1 Selected bond length (Å) and angles (°) for complexes **1–4**

1	**2**	**3**	**4**
Eu(1)–O(1) 2.383(3)	Eu(1)–O(1) 2.343(4)	Sm(1)–O(1) 2.397(3)	Sm(1)–O(1) 2.357(4)
Eu(1)–O(2) 2.408(4)	Eu(1)–O(2) 2.381(4)	Sm(1)–O(2) 2.414(4)	Sm(1)–O(2) 2.398(4)
Eu(1)–O(5) 2.376(3)	Eu(1)–O(5) 2.381(4)	Sm(1) –O(5) 2.390(3)	Sm(1)–O(5) 2.391(4)
Eu(1)–O(6) 2.365(3)	Eu(1)–O(6) 2.415(4)	Sm(1) –O(6) 2.374(3)	Sm(1)–O(6) 2.422(4)
Eu(1)–O(9) 2.362(4)	Eu(1)–O(9) 2.399(4)	Sm(1) –O(9) 2.384(3)	Sm(1)–O(9) 2.407(4)
Eu(1)–O(10) 2.445(3)	Eu(1)–O(10) 2.361(4)	Sm(1)–O(10) 2.462(3)	Sm(1)–O(10) 2.377(4)
Eu(1)–O(13) 2.458(3)	Eu(1)–N(4) 2.607(5)	Sm(1)–O(13) 2.470(3)	N(4)–Sm(1) 2.618(5)
Eu(1)–O(14) 2.449(3)	Eu(1)–N(5) 2.618(5)	Sm(1) –O(14) 2.459(3)	N(5)–Sm(1) 2.636(5)
O(1)–Eu(1)–O(2) 72.24(11)	O(1)–Eu(1)–O(2) 72.22(14)	O(1)–Sm (1)–O(2) 71.69(11)	O(1)–Sm (1)–O(2) 71.84(13)
O(5)–Eu(1)–O(6). 73.51(12)	O(5)–Eu(1)–O(6) 71.79(14)	O(5)–Sm (1)–O(6). 73.29(12)	O(5)–Sm (1)–O(6) 71.77(13)
O(9)–Eu(1)–O(10) 73.63(11)	O(9)–Eu(1)–O(10) 72.36(14)	O(9)–Sm (1)–O(10) 73.26(11)	O(9)–Sm (1)–O(10) 72.07(13)
O(13)–Eu(1)–O(14) 144.72(12)	N(4)–Eu(1)–N(5) 62.83(16)	O(13)–Sm(1)–O(14) 145.05(11)	N(4)–Sm(1)–N(5) 62.57(15)